AIMS Mathematics, 11(5): 13632–13646.
DOI: 10.3934/math.2026561
Received: 06 March 2026
Revised: 15 April 2026
Accepted: 24 April 2026
Published: 15 May 2026

https://www.aimspress.com/journal/Math

Research article

Finite difference approach to solving the heat equation with purely integral conditions

Ouarda Benmanseur[1,2], Ahcene Merad[2,*], Hadjer Zerouali[2], and Dhouha Saadi[2]

[1] Laboratory of Knowledge Engineering and Computer Security, Department of Mathematics, Khenchela University Abbes Laghrour, Algeria

[2] Laboratory of Dynamical Systems and Control, Department of Mathematics, Oum El Bouaghi University Larbi Ben Mhidi, Algeria

* **Correspondence:** Email: ahcene.merad@univ-oeb.dz.

Abstract: We study an explicit finite difference approximation for the one-dimensional heat equation with purely integral conditions. The integral constraints are discretized by the trapezoidal rule, which yields explicit formulas for the boundary values at each time level and leads to a dense iteration matrix for the interior unknowns. The scheme is written in matrix form, its local truncation error is estimated, and a stability-convergence statement is established under a natural power-boundedness assumption on the full iteration matrix. Numerical experiments are reported for both stable and unstable time steps. In particular, a fixed-final-time convergence study confirms the expected first-order behavior with respect to the time step when k and h^2 are refined simultaneously. The paper also documents the larger errors observed near the first and last interior nodes, a characteristic feature of the boundary reconstruction induced by the integral conditions.

Keywords: heat equation; purely integral conditions; explicit finite difference scheme; stability; convergence; nonlocal conditions
Mathematics Subject Classification: 35K05, 65M06, 65M12

1. Introduction

Parabolic problems with nonlocal constraints arise when the state is not prescribed pointwise at the boundary but through global measurements such as total mass, weighted moments, or energy balance relations. Such formulations appear in heat conduction, thermoelasticity, ion transport, and diffusion in heterogeneous media. Early analytical studies by Day [6, 7] and Friedman [11] showed that nonlocal conditions may substantially alter the qualitative behavior of parabolic solutions, while related solvability questions for equations with integral constraints and fractional/nonlocal models

were also investigated in other settings; see, for instance, [4, 19].

From the numerical point of view, the heat equation with nonlocal or integral conditions has been treated by several families of methods. General explicit and stable finite-difference/time-integration schemes for heat and diffusion-type equations are discussed in [14, 15, 17]. Ekolin [10] analyzed forward Euler, backward Euler, and Crank–Nicolson discretizations for the one-dimensional heat equation with integral boundary conditions. Finite element and Galerkin-type approaches were later developed by Fairweather and López-Marcos [12] and by Bouziani, Merazga, and Benamira [3]. Monotone and weighted finite-difference schemes for parabolic problems with nonlocal conditions were investigated in [2, 5, 16]. For two-dimensional diffusion problems with integral constraints, implicit, explicit, and splitting strategies were studied by Dehghan [8, 9], Sapagovas and Jesevičiūtė [22], Sapagovas [23], and Sajavičius [20, 21]. Recent works continue to examine explicit, implicit, and nonlinear variants of nonlocal heat models [1, 13, 24].

Despite this progress, comparatively little attention has been given to a fully explicit treatment of the one-dimensional heat equation with two purely integral conditions of the form (1.3) and (1.4). In this setting, the boundary values are not prescribed independently; instead, they must be reconstructed at every time level from the integral data. This reconstruction couples the first and last interior equations with all interior unknowns, so the explicit iteration is no longer tridiagonal. Understanding how this dense coupling influences stability and error propagation is therefore essential.

The present work revisits the problem studied in [18] and gives a corrected and more transparent explicit finite-difference formulation. The main contributions are as follows. First, we derive the boundary reconstruction formulas obtained from the trapezoidal discretization of the two integral constraints and write the full method in matrix form. Second, we establish consistency and a stability-convergence statement based on the power-boundedness of the complete iteration matrix, which is the natural matrix-spectral framework used in the analysis of nonlocal schemes [20–23]. Third, we provide a more detailed interpretation of the numerical evidence: we relate the spectral radius to the observed stable and unstable regimes, explain why the largest errors concentrate near the first and last interior nodes, and verify the fixed-final-time convergence trend predicted by the theoretical estimate.

We consider the problem

$$U_l(s,l) - \alpha U_{ss}(s,l) = F(s,l), \qquad 0 < s < 1,\ 0 < l \le \Gamma, \tag{1.1}$$

$$U(s,0) = \phi(s), \qquad 0 < s < 1, \tag{1.2}$$

$$\int_0^1 U(s,l)\,ds = \psi_1(l), \qquad 0 < l \le \Gamma, \tag{1.3}$$

$$\int_0^1 s\,U(s,l)\,ds = \psi_2(l), \qquad 0 < l \le \Gamma. \tag{1.4}$$

Here U denotes the temperature, ϕ, ψ_1, ψ_2, and F are known functions, and $\alpha > 0$, $\Gamma > 0$ are constants. We keep the notation (s, l), which is consistent with [18]. Throughout the paper, subscript notation denotes partial derivatives; for example, $U_l = \partial U/\partial l$ and $U_{ss} = \partial^2 U/\partial s^2$.

The rest of the paper is organized as follows. Section 2 derives the explicit scheme and the reconstructed boundary values. Section 3 gives the matrix formulation. Section 4 discusses consistency, stability, and convergence. Section 5 contains numerical experiments, including a

fixed-final-time convergence study and additional tests with different parameter values. A MATLAB implementation is included in Appendix A.

2. Discretization of the problem

Let $N, M \in \mathbb{N}$, $h = 1/N$, and $k = \Gamma/M$. We define

$$s_i = ih, \qquad i = 0, 1, \ldots, N, \qquad l_n = nk, \qquad n = 0, 1, \ldots, M.$$

We denote by U_i^n an approximation of $U(s_i, l_n)$ and set $F_i^n = F(s_i, l_n)$, $\psi_r^n = \psi_r(l_n)$ for $r = 1, 2$.

Applying a forward Euler discretization in time and a centered difference in space gives

$$\frac{U_i^{n+1} - U_i^n}{k} - \alpha \frac{U_{i-1}^n - 2U_i^n + U_{i+1}^n}{h^2} = F_i^n, \qquad i = 1, \ldots, N-1, \quad n = 0, \ldots, M-1. \tag{2.1}$$

Hence

$$U_i^{n+1} = \lambda U_{i-1}^n + (1 - 2\lambda)U_i^n + \lambda U_{i+1}^n + kF_i^n, \qquad \lambda = \frac{\alpha k}{h^2}. \tag{2.2}$$

The initial data are discretized as

$$U_i^0 = \phi(s_i), \qquad i = 1, \ldots, N-1. \tag{2.3}$$

The integral conditions are approximated by the trapezoidal rule:

$$\psi_1^n = \frac{h}{2}\left(U_0^n + U_N^n + 2\sum_{i=1}^{N-1} U_i^n\right), \tag{2.4}$$

$$\psi_2^n = \frac{h}{2}\left(U_N^n + 2h\sum_{i=1}^{N-1} iU_i^n\right), \qquad n = 0, \ldots, M. \tag{2.5}$$

This choice is standard in finite-difference treatments of nonlocal heat problems because it preserves simple linear reconstruction formulas for the unknown boundary values [2, 10, 16]. Solving (2.4) and (2.5) for the boundary values yields

$$U_N^n = \frac{2\psi_2^n}{h} - 2h\sum_{j=1}^{N-1} jU_j^n, \tag{2.6}$$

$$U_0^n = \frac{2(\psi_1^n - \psi_2^n)}{h} + 2\sum_{j=1}^{N-1}(jh - 1)U_j^n. \tag{2.7}$$

These relations make the method explicit: once the interior vector U^n is known, both boundary values are computed directly, after which (2.2) provides the next time level.

Substituting (2.7) and (2.6) into (2.2) gives the near-boundary equations

$$U_1^{n+1} = (2\lambda(h-1) + (1-2\lambda))U_1^n + (2\lambda(2h-1) + \lambda)U_2^n + 2\lambda\sum_{j=3}^{N-1}(jh-1)U_j^n$$

$$+\frac{2\lambda}{h}(\psi_1^n-\psi_2^n)+kF_1^n, \tag{2.8}$$

$$U_{N-1}^{n+1}=(\lambda-2\lambda(N-2)h)U_{N-2}^n+((1-2\lambda)-2\lambda(N-1)h)U_{N-1}^n-2\lambda h\sum_{j=1}^{N-3}jU_j^n$$

$$+\frac{2\lambda}{h}\psi_2^n+kF_{N-1}^n. \tag{2.9}$$

For the interior nodes $i=2,\dots,N-2$, (2.2) remains the standard three-point explicit stencil.

3. Matrix formulation

Let

$$U^n=(U_1^n,U_2^n,\dots,U_{N-1}^n)^T,\qquad F^n=(F_1^n,F_2^n,\dots,F_{N-1}^n)^T.$$

We also define

$$S^n=\left(\frac{2\lambda}{h}(\psi_1^n-\psi_2^n),\,0,\dots,0,\,\frac{2\lambda}{h}\psi_2^n\right)^T,\qquad L^n=S^n+kF^n.$$

Then the scheme can be written as

$$U^{n+1}=MU^n+L^n,\qquad n=0,1,\dots,M-1, \tag{3.1}$$

where $M=(m_{ij})_{1\le i,j\le N-1}$ is the dense matrix defined by

$$\begin{aligned}
m_{1,1}&=2\lambda(h-1)+(1-2\lambda),\\
m_{1,2}&=2\lambda(2h-1)+\lambda,\\
m_{1,j}&=2\lambda(jh-1),\qquad j=3,\dots,N-1,\\
m_{N-1,N-2}&=\lambda-2\lambda(N-2)h,\\
m_{N-1,N-1}&=(1-2\lambda)-2\lambda(N-1)h,\\
m_{N-1,j}&=-2\lambda hj,\qquad j=1,\dots,N-3,
\end{aligned}$$

and, for $2\le i\le N-2$,

$$m_{i,i-1}=\lambda,\qquad m_{i,i}=1-2\lambda,\qquad m_{i,i+1}=\lambda,$$

with all other entries equal to zero.

Equation (3.1) makes the influence of the integral conditions explicit: the first and last rows are dense, while the interior rows remain tridiagonal. A similar "tridiagonal core plus dense boundary rows" structure also appears in weighted and θ-type discretizations for nonlocal heat problems [2,5,16]. Since the method is explicit, advancing one time step only requires the multiplication of M by the current state vector and the addition of L^n.

4. Consistency, stability, and convergence

4.1. Consistency

Proposition 1. *Assume that $U\in C^{4,2}([0,1]\times[0,\Gamma])$. Then the local truncation error $R_i^{(n)}$ of (2.1) satisfies*

$$|R_i^{(n)}|\le C(k+\alpha h^2),\qquad i=1,\dots,N-1,\quad n=0,\dots,M-1, \tag{4.1}$$

for some constant C independent of h and k.

Proof. A Taylor expansion in time gives

$$U_l(s_i, l_n) = \frac{U(s_i, l_{n+1}) - U(s_i, l_n)}{k} - \frac{k}{2} U_{ll}(s_i, \theta_n),$$

for some $\theta_n \in (l_n, l_{n+1})$. Likewise, a Taylor expansion in space yields

$$U_{ss}(s_i, l_n) = \frac{U(s_{i-1}, l_n) - 2U(s_i, l_n) + U(s_{i+1}, l_n)}{h^2} - \frac{h^2}{12} U_{ssss}(\xi_i, l_n),$$

for some $\xi_i \in (s_{i-1}, s_{i+1})$. Substituting these expressions into (1.1) and comparing with (2.1) proves (4.1). □

4.2. Stability

The classical explicit restriction $\lambda \leq 1/2$ remains the relevant threshold for the present problem. However, due to the elimination of the boundary values through (2.7) and (2.6), the full iteration matrix is dense and the standard maximum-principle proof for the three-point stencil no longer applies directly. Following the matrix-spectral viewpoint adopted in [20–23], we therefore formulate stability in terms of the powers of the complete transition matrix.

Proposition 2. *Let the full scheme be written as* (3.1)*. Assume that $0 \leq \lambda \leq 1/2$ and that the powers of M are uniformly bounded in the infinity norm, that is,*

$$\|M^n\|_\infty \leq C_M \qquad \text{for all } n \geq 0,$$

with a constant C_M independent of n. Then the scheme is stable in $\|\cdot\|_\infty$.

Proof. Consider two numerical solutions of (3.1) generated from different initial vectors but with the same data L^n. Their difference E^n satisfies

$$E^{n+1} = ME^n.$$

Hence

$$E^n = M^n E^0, \qquad \|E^n\|_\infty \leq \|M^n\|_\infty \|E^0\|_\infty \leq C_M \|E^0\|_\infty.$$

Therefore perturbations in the initial data remain uniformly bounded for all time levels. □

Remark 3. *For the matrices used in Section 5, the computed spectral radius satisfies $\rho(M) < 1$ whenever $\lambda < 1/2$, whereas $\rho(M) > 1$ when $\lambda > 1/2$. This is consistent with the observed blow-up for the unstable cases in Figure 1 and Table 1.*

Table 1. Spectral radius and error summary for $n = 7$, $h = 0.05$, and $\alpha = 1$.

k	λ	$\rho(M)$	$\|e\|_\infty$	$\|e\|_2$
0.0025	1.0000	3.000000	1.588708e+01	7.147506e+00
0.0016	0.6400	1.560000	1.509848e-01	7.019799e-02
0.001	0.4000	0.960845	7.978429e-03	4.405654e-03
0.0001	0.0400	0.996085	9.329870e-03	3.061557e-03
1e-05	0.0040	0.999608	1.408409e-03	4.573229e-04
1e-06	0.0004	0.999961	1.468638e-04	4.767724e-05

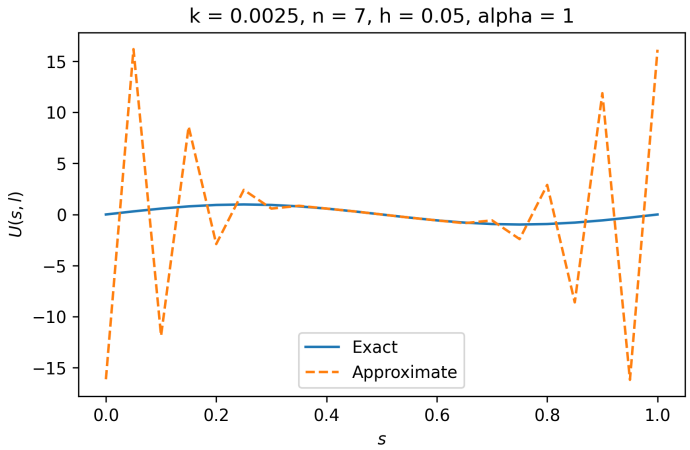

Figure 1. Exact and approximate solutions for $k = 0.0025$, $n = 7$, $h = 0.05$, and $\alpha = 1$. Here $\lambda = 1 > 1/2$, so the scheme is unstable.

4.3. Convergence

Theorem 4. *Assume the hypotheses of the previous proposition and the truncation estimate* (4.1). *Let*

$$e_i^n = U(s_i, l_n) - U_i^n, \qquad i = 1, \ldots, N-1.$$

Then, for $l_n = nk \le \Gamma$,

$$\|e^n\|_\infty \le C_M \|e^0\|_\infty + \Gamma C_M C(k + \alpha h^2). \tag{4.2}$$

In particular, if the initial condition is imposed exactly, then the scheme converges as $(h, k) \to (0, 0)$.

Proof. Let R^n be the vector of local truncation errors. Subtracting the numerical scheme from the exact discrete identity gives

$$e^{n+1} = Me^n + kR^n.$$

Iterating this recursion yields

$$e^n = M^n e^0 + k \sum_{j=0}^{n-1} M^{n-1-j} R^j.$$

Taking infinity norms and using $\|R^j\|_\infty \le C(k + \alpha h^2)$ together with the power-boundedness of M gives

$$\|e^n\|_\infty \le C_M \|e^0\|_\infty + k \sum_{j=0}^{n-1} C_M C(k + \alpha h^2) \le C_M \|e^0\|_\infty + nk\, C_M C(k + \alpha h^2).$$

Since $nk = l_n \le \Gamma$, estimate (4.2) follows. □

5. Numerical experiments

We test the scheme on

$$U_l(s, l) - \alpha U_{ss}(s, l) = \frac{(-1 + 4\pi^2 \alpha(1 + l)) \sin(2\pi s)}{(1 + l)^2}, \qquad 0 < s < 1,\ 0 < l \le \Gamma, \tag{5.1}$$

$$U(s,0) = \sin(2\pi s), \tag{5.2}$$

$$\int_0^1 U(s,l)\,ds = 0, \tag{5.3}$$

$$\int_0^1 sU(s,l)\,ds = -\frac{1}{2\pi(1+l)}. \tag{5.4}$$

The exact solution is

$$U(s,l) = \frac{\sin(2\pi s)}{1+l}.$$

Unless stated otherwise, we use $h = 0.05$ ($N = 20$). All reported errors are computed at the interior nodes s_i, $i = 1, \ldots, N-1$, because the boundary values are reconstructed from the integral conditions and are not prescribed pointwise. The reconstruction step explains why the largest pointwise errors occur near the first and last interior nodes.

5.1. Stable and unstable time steps

Table 1 summarizes the behavior of the method for $n = 7$ time steps. The unstable cases $k = 0.0025$ and $k = 0.0016$ violate the condition $\lambda \le 1/2$; correspondingly, the computed spectral radius of the full iteration matrix exceeds 1 and large errors appear. For $k \le 10^{-3}$, the method is stable and the errors become small. This behavior is consistent with the spectral-stability analyses reported for related nonlocal schemes in [20–23]. Figure 1 clearly shows the blow-up when $\lambda = 1$, while Figures 2–5 show the agreement between the numerical and exact solutions for stable time steps.

The figures also reveal a more nuanced transition toward stability. In Figure 2, where $\lambda = 0.64$, the interior part of the profile still follows the correct oscillatory shape, but visible distortions remain near the first and last interior nodes. In Figure 3 the numerical and exact curves are already close over the whole interval, and the discrepancy continues to decrease in Figures 4 and 5. Figure 6 confirms that, for $k = 10^{-6}$, the remaining pointwise difference is below the graphical resolution on the displayed subinterval. Thus, the visual evidence is fully consistent with the spectral-radius indicator reported in Table 1.

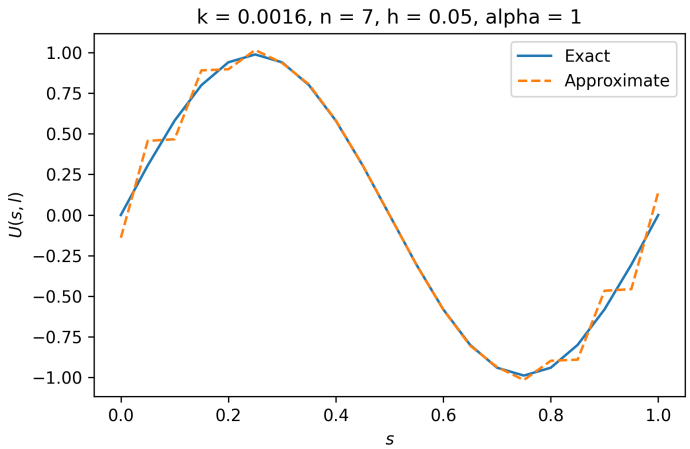

Figure 2. Exact and approximate solutions for $k = 0.0016$, $n = 7$, $h = 0.05$, and $\alpha = 1$.

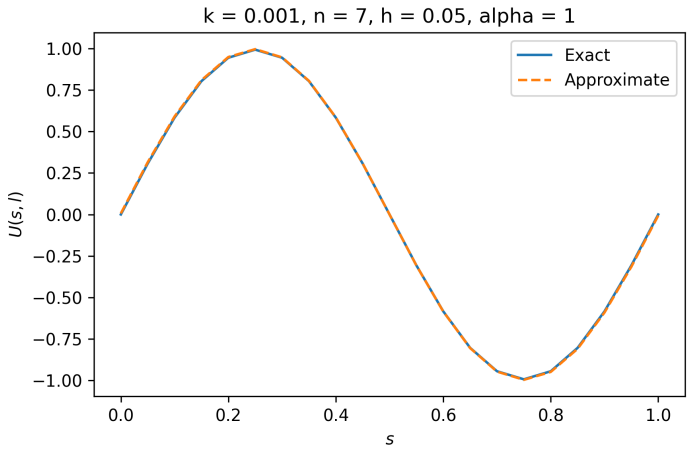

Figure 3. Exact and approximate solutions for $k = 0.001$, $n = 7$, $h = 0.05$, and $\alpha = 1$.

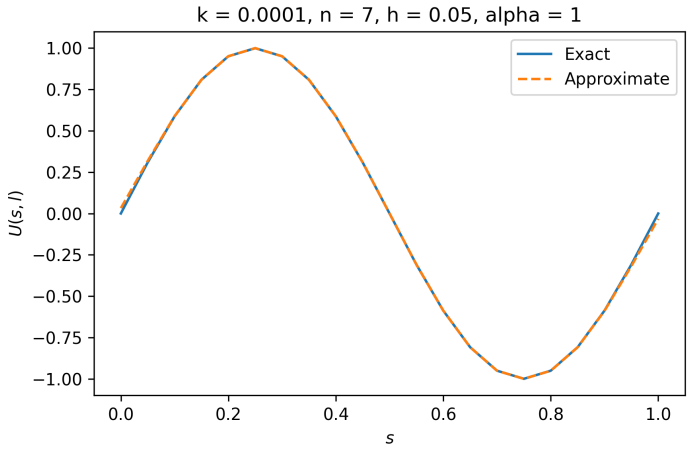

Figure 4. Exact and approximate solutions for $k = 10^{-4}$, $n = 7$, $h = 0.05$, and $\alpha = 1$.

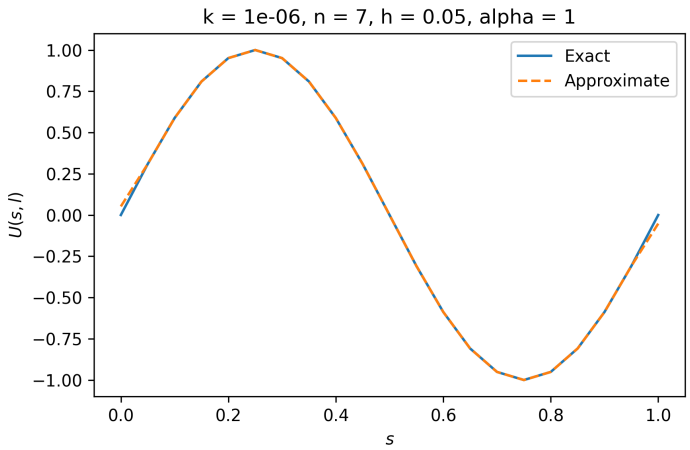

Figure 5. Exact and approximate solutions for $k = 10^{-6}$, $n = 7$, $h = 0.05$, and $\alpha = 1$.

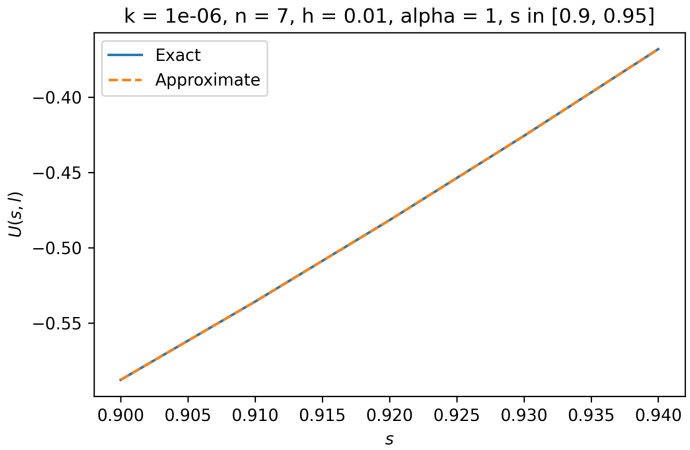

Figure 6. Zoom of the solution profile on $[0.9, 0.95]$ for $k = 10^{-6}$. The numerical and exact curves are visually indistinguishable at this scale.

5.2. Boundary error behavior

Table 2 reports the absolute error at selected nodes for three stable time steps. The largest errors occur at $s = 0.05$ and $s = 0.95$, i.e. the first and last interior nodes, which are the most directly affected by the reconstructed boundary values. As k decreases, these errors decay rapidly.

Table 2. Absolute error at selected interior nodes for $n = 7$, $h = 0.05$, and $\alpha = 1$.

s	$k = 10^{-4}$	$k = 10^{-5}$	$k = 10^{-6}$
0.05	9.329870e-03	1.408409e-03	1.468638e-04
0.10	1.315452e-03	3.024071e-05	1.506940e-06
0.25	2.238567e-04	2.262617e-05	2.265135e-06
0.50	9.068304e-17	1.138669e-17	1.218203e-18
0.75	2.238567e-04	2.262617e-05	2.265135e-06
0.90	1.315452e-03	3.024071e-05	1.506940e-06
0.95	9.329870e-03	1.408409e-03	1.468638e-04

The table also shows that the localization of the error is not accidental. For $k = 10^{-4}$, the error at $s = 0.05$ is about one order of magnitude larger than at $s = 0.10$, and the same pattern appears symmetrically near $s = 0.95$. By contrast, the error at the midpoint $s = 0.50$ is essentially at machine precision because the exact solution vanishes there. This concentration of the maximum error near the first and last interior nodes is consistent with earlier observations for one-dimensional nonlocal heat schemes, where the elimination of boundary values creates dense couplings in the extreme rows of the discrete operator [2, 10, 16].

5.3. Convergence for fixed final time

To avoid the ambiguity that comes from fixing the number of time steps, we next fix the final time at $T = 0.01$. We refine the mesh with a fixed CFL ratio $\lambda = 0.2$, i.e. $k = 0.2h^2$. Table 3 shows a first-order convergence rate with respect to k, in agreement with the estimate (4.2).

This interpretation is important because, under the refinement law $k = 0.2h^2$, the theoretical bound $O(k + h^2)$ reduces to $O(k)$. The rates in Table 3 are therefore not merely descriptive; they verify that the dominant error behaves exactly as predicted by the consistency and stability analysis. In particular, the nearly constant halving pattern in the maximum norm confirms that the explicit reconstruction of the boundary values does not destroy the global convergence order when the full matrix remains stable.

Table 3. Fixed-final-time convergence study for $T = 0.01$ with $\lambda = 0.2$ and $\alpha = 1$.

N	h	k	$\|e(T)\|_\infty$	rate
20	0.05000	0.00050000	6.771805e-03	–
40	0.02500	0.00012500	1.690152e-03	1.001
80	0.01250	0.00003125	4.232731e-04	0.999
160	0.00625	0.00000781	1.057870e-04	1.000

5.4. Additional tests

Tables 4 and 5 provide additional results for $n = 9$ time steps with two values of α. When $\alpha = 1$, the L^2 error decreases monotonically as k decreases, while the L^∞ norm remains more sensitive to the first and last interior nodes. When $\alpha = 0.03$, the stability parameter λ is much smaller, and both error norms decay smoothly.

Table 4. Additional tests for $n = 9$, $h = 0.05$, and $\alpha = 1$.

k	λ	$\|e\|_\infty$	$\|e\|_2$
0.0016	0.6400	3.126416e-01	1.578361e-01
0.001	0.4000	6.880802e-03	4.479326e-03
0.0005	0.2000	9.840975e-03	4.359468e-03
0.0001	0.0400	1.043873e-02	3.450735e-03
1e-05	0.0040	1.783163e-03	5.790759e-04
1e-06	0.0004	1.885322e-04	6.120465e-05

Table 5. Additional tests for $n = 9$, $h = 0.05$, and $\alpha = 0.03$.

k	λ	$\|e\|_\infty$	$\|e\|_2$
0.0016	0.019200	6.746543e-03	2.199110e-03
0.001	0.012000	4.712246e-03	1.532448e-03
0.0005	0.006000	2.588009e-03	8.406231e-04
0.0001	0.001200	5.583791e-04	1.812784e-04
1e-05	0.000120	5.680351e-05	1.844024e-05
1e-06	0.000012	5.690107e-06	1.847182e-06

These two tables clarify the role of the diffusion coefficient in the explicit stability parameter. For $\alpha = 1$, moderate values of k still produce a visible endpoint effect in the maximum norm, so $\|e\|_\infty$ is not strictly monotone for all stable time steps. This does not contradict convergence; it only indicates that the largest error is governed by the boundary-reconstruction mechanism. By contrast, when $\alpha = 0.03$, the quantity $\lambda = \alpha k/h^2$ is sufficiently small across the whole experiment, and the numerical errors

decay in a smoother and more uniform fashion. In other words, the tables separate two phenomena: the intrinsic consistency of the scheme and the additional sensitivity introduced by the nonlocal boundary reconstruction when λ is closer to the stability threshold.

Finally, Figures 7 and 8 compare the exact and approximate solution surfaces on the interval $0 \leq l \leq 0.01$. The two surfaces are in very good agreement.

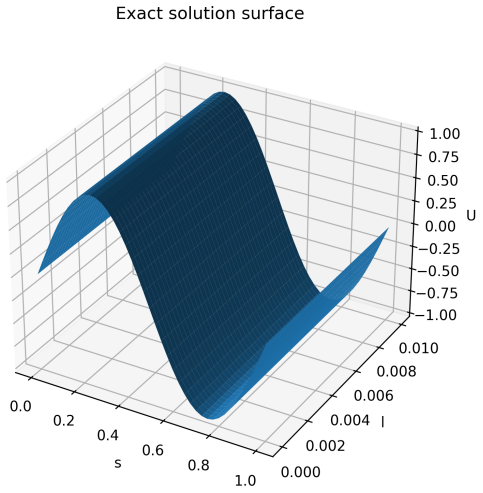

Figure 7. Exact solution surface for (5.1)–(5.4) on $0 \leq l \leq 0.01$.

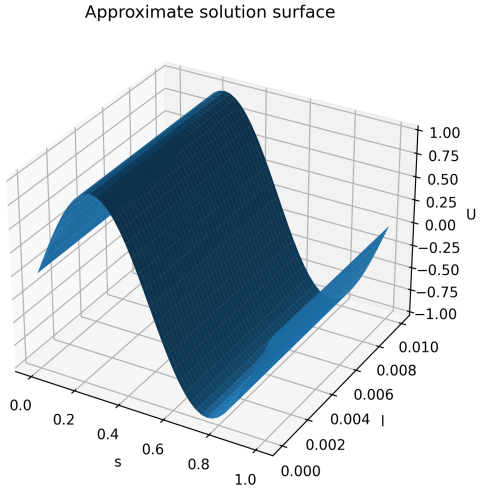

Figure 8. Approximate solution surface computed with $N = 80$, $\lambda = 0.2$, and $T = 0.01$.

This agreement is meaningful for two reasons. First, the numerical surface reproduces both the amplitude decay in time and the oscillatory spatial structure of the exact solution, so the match is not limited to isolated cross-sections. Second, the absence of visible distortion near the lateral edges of the surface indicates that the boundary reconstruction remains accurate over the entire time interval when the CFL ratio is kept in the stable regime. Therefore the surface plots complement Tables 3–5 by providing a global space-time verification of the method.

6. Conclusions

We have presented an explicit finite-difference treatment of the one-dimensional heat equation with two purely integral conditions and rewritten the method in a form that makes the nonlocal coupling completely explicit. The discrete integral constraints lead to closed formulas for the boundary values, but they also transform the standard tridiagonal explicit heat operator into a dense matrix in the first and last rows. This is the main structural feature of the problem and it explains both the usefulness and the limitations of the method.

From the analytical viewpoint, the scheme is consistent with local truncation error $O(k + \alpha h^2)$. Stability is naturally expressed through the power-boundedness of the full iteration matrix, and in the numerical tests this framework is fully compatible with the practical threshold $\lambda \leq 1/2$. From the computational viewpoint, the method is attractive because each time step is inexpensive and requires no linear solve, so it provides a transparent benchmark for studying the effect of the integral conditions.

The numerical results support three clear conclusions. First, the spectral radius of the iteration matrix accurately distinguishes stable and unstable parameter choices. Second, when the scheme is stable, the dominant pointwise errors are localized near the first and last interior nodes, precisely where the reconstructed boundary data enter the stencil. Third, under the refinement law $k \propto h^2$, the fixed-final-time experiments recover the expected first-order behavior with respect to k, in agreement with the convergence estimate.

Therefore, the revised manuscript does not merely report an explicit algorithm; it clarifies the discrete structure induced by the integral conditions, connects the observed behavior to matrix-spectral stability, and documents the regimes in which the method is reliable. A natural continuation of this work would be to study implicit or IMEX variants, higher-order quadrature for the integral constraints, and sharper stability criteria that remove the power-boundedness assumption from the convergence theorem.

Author contributions

The authors contributed equally to this work. All authors participated in the development of the results, the preparation of the manuscript, and the approval of the final version.

Use of Generative-AI tools declaration

The authors declare that they have not used Artificial Intelligence (AI) tools in the creation of this article.

Acknowledgments

The authors would like to thank the reviewers for their valuable comments and constructive suggestions, which helped improve the quality and presentation of this paper.

Conflict of interest

The authors declare that there is no conflict of interest.

References

1. S. Bensaid, S. Dehilis, A. Bouziani, Explicit and implicit Crandall's scheme for the heat equation with nonlocal nonlinear conditions, *Int. J. Anal. Appl.*, **19** (2021), 660–673. https://doi.org/10.28924/2291-8639-19-2021-660
2. N. Borovykh, Stability in the numerical solution of the heat equation with nonlocal boundary conditions, *Appl. Numer. Math.*, **42** (2002), 17–27. https://doi.org/10.1016/S0168-9274(01)00139-8
3. A. Bouziani, N. Merazga, S. Benamira, Galerkin method applied to a parabolic evolution problem with nonlocal boundary conditions, *Nonlinear Anal.*, **69** (2008), 1515–1524. https://doi.org/10.1016/j.na.2007.07.008
4. S. Brahimi, A. Merad, K. Kilicman, Theoretical and numerical aspect of fractional differential equations with purely integral conditions, *Mathematics*, **9** (2021), 1987. https://doi.org/10.3390/math9161987
5. R. Čiegis, A. Štikonas, O. Štikonienė, O. Suboč, A monotonic finite-difference scheme for a parabolic problem with nonlocal conditions, *Diff. Equ.*, **38** (2002), 1027–1037. https://doi.org/10.1023/A:1021167932414
6. W. A. Day, Extensions of a property of the heat equation to linear thermoelasticity and other theories, *Quart. Appl. Math.*, **40** (1982), 319–330. https://doi.org/10.1090/qam/678203
7. W. A. Day, A decreasing property of solutions of parabolic equations with applications to thermoelasticity, *Quart. Appl. Math.*, **41** (1983), 468–475. https://doi.org/10.1090/qam/693879
8. M. Dehghan, Implicit locally one-dimensional methods for two-dimensional diffusion with a non-local boundary condition, *Math. Comput. Simul.*, **49** (1999), 331–349. https://doi.org/10.1016/S0378-4754(99)00056-7
9. M. Dehghan, Fully explicit finite-difference methods for two-dimensional diffusion with an integral condition, *Nonlinear Anal.*, **48** (2002), 637–650. https://doi.org/10.1016/S0362-546X(00)00172-3
10. G. Ekolin, Finite difference methods for a nonlocal boundary value problem for the heat equation, *BIT*, **31** (1991), 245–261. https://doi.org/10.1007/BF01931285
11. A. Friedman, Monotonic decay of solutions of parabolic equations with nonlocal boundary conditions, *Quart. Appl. Math.*, **44** (1986), 401–407. https://doi.org/10.1090/qam/860893
12. G. Fairweather, J. C. López-Marcos, Galerkin methods for a semilinear parabolic problem with nonlocal boundary conditions, *Adv. Comput. Math.*, **6** (1996), 243–262. https://doi.org/10.1007/BF02127706
13. Z. Hammouch, A. Zahra, A. Rehman, S. A. Mardan, An efficient numerical technique for solving heat equation with nonlocal boundary conditions, *Adv. Theory Nonlinear Anal. Appl.*, **6** (2022), 157–167. https://doi.org/10.31197/atnaa.846217
14. H. K. Jalghaf, E. Kovács, J. Majár, Á. Nagy, A. H. Askar, Explicit stable finite difference methods for diffusion-reaction type equations, *Mathematics*, **9** (2021), 3308. https://doi.org/10.3390/math9243308

15. H. K. Jalghaf, I. Omle, E. Kovács, A comparative study of explicit and stable time integration schemes for heat conduction in an insulated wall, *Buildings*, **12** (2022), 824. https://doi.org/10.3390/buildings12060824
16. Y. Liu, Numerical solution of the heat equation with nonlocal boundary conditions, *J. Comput. Appl. Math.*, **110** (1999), 115–127. https://doi.org/10.1016/S0377-0427(99)00200-9
17. W. Z. Loskor, R. Sarkar, A numerical solution of heat equation for several thermal diffusivity using finite difference scheme with stability conditions, *J. Appl. Math. Phys.*, **10** (2022), 449–465. https://doi.org/10.4236/jamp.2022.102034
18. A. Merad, A. Bouziani, Numerical solution for parabolic equation with nonlocal conditions, *TJMM*, **5** (2013), 121–127.
19. L. S. Pulḱina, The L^2 solvability of a nonlocal problem with integral conditions for a hyperbolic equation, *Differ. Equ.*, **36** (2000), 316–318. https://doi.org/10.1007/BF02754219
20. S. Sajavičius, On the stability of fully-explicit finite-difference scheme for two-dimensional parabolic equation with nonlocal conditions, In: *Computational Science and Its Applications-ICCSA 2011, Berlin: Springer*, 2011. https://doi.org/10.1007/978-3-642-21898-9_1
21. S. Sajavičius, Stability of the weighted splitting finite-difference scheme for a two-dimensional parabolic equation with two nonlocal integral conditions, *Comput. Math. Appl.*, **64** (2012), 3485–3499. https://doi.org/10.1016/j.camwa.2012.08.009
22. M. Sapagovas, Z. Jeseviciute, On the stability of finite-difference schemes for parabolic equations subject to integral conditions with applications to thermoelasticity, *Comput. Meth. Appl. Math.*, **8** (2008), 360–373.
23. M. Sapagovas, On the stability of a finite-difference scheme for nonlocal parabolic boundary-value problems, *Lith. Math. J.*, **48** (2008), 339–356. https://doi.org/10.1007/s10986-008-9017-5
24. Y. Zhou, M. Cui, Y. Lin, Numerical algorithm for parabolic problems with non-classical conditions, *J. Comput. Appl. Math.*, **230** (2009), 770–780. https://doi.org/10.1016/j.cam.2009.01.012

A. MATLAB code

For reproducibility we include a compact MATLAB implementation of the corrected scheme.

```
function [s,U] = heat_integral_explicit(N,k,Gamma,alpha)
% Explicit finite-difference solver for the heat equation
% U_l - alpha U_ss = F(s,l)
% with purely integral conditions
%
% int_0^1 U(s,l) ds     = psi1(l),
% int_0^1 s U(s,l) ds   = psi2(l).

h = 1/N;
M = round(Gamma/k);
s = linspace(0,1,N+1).';
U = sin(2*pi*s);          % initial condition phi(s)
```

```
for n = 0:M-1
    l = n*k;
    idx = (1:N-1).';

    % Boundary values reconstructed from the integral conditions
    UN = 2*psi2(l)/h - 2*h*sum(idx .* U(2:N));
    U0 = 2*(psi1(l)-psi2(l))/h + 2*sum((idx*h-1) .* U(2:N));

    Ufull = U;
    Ufull(1)   = U0;
    Ufull(end) = UN;

    lam = alpha*k/h^2;
    Unext = U;

    for i = 2:N
        Unext(i) = lam*Ufull(i-1) + (1-2*lam)*Ufull(i) + ...
                   lam*Ufull(i+1) + k*F(s(i),l,alpha);
    end

    U = Unext;
end
end

function val = F(s,l,alpha)
val = ((-1 + 4*pi^2*alpha*(1+l))*sin(2*pi*s))/((1+l)^2);
end

function val = psi1(~)
val = 0;
end

function val = psi2(l)
val = -1/(2*pi*(1+l));
end
```